SF2A 2025
A. Siebert, K. Baillié, M. Béthermin, F. Cantalloube, E. Josselin, N. Lagarde, J. Malzac, J. Richard, L. Selliez, O. Venot (eds)

NEW BRANCH OF THE TAYLER-SPRUIT DYNAMO IN 3D NUMERICAL SIMULATIONS OF STABLY STRATIFIED STELLAR REGIONS

P. Barrère[1], A. Reboul-Salze[2], P. Eggenberger[1], C. Rodriguez[1] and M. Marchand[1]

Abstract. The Tayler-Spruit dynamo is a promising candidate of transport mechanism to explain the slow stellar core rotations observed by asteroseismology. Despite a few analytical works, this dynamo remains poorly known due to its very recent identification in direct numerical simulations. We report the existence of another solution of this dynamo for stellar radiative regions, which is maintained at strong stratifications for the first time. This new branch is in bistability with the dynamo identified by Petitdemange et al. at low stratifications, but the turbulence occurs mostly near the polar axis instead of the equator. The scaling law for the transport is consistent with the revised model of Fuller et al., even though slightly less efficient. Finally, the asteroseismic asymmetry parameter of the new branch remains close to 1 while it is around -0.5 for the other, predicting a variety of values consistent with current observations.

Keywords: stars: magnetic field, stars: rotation, numerical simulations, MHD, dynamo

1 Introduction

The advent asteroseismology has provided the first observational constrains on the internal rotation of (mostly low-mass) main-sequence and evolved stars (e.g. Gehan et al. 2018; Li et al. 2020, 2024). They reveal that the stellar cores rotate several order of magnitudes slower than predicted by stellar evolution models that only include the effects of hydrodynamic instabilities and meridional circulation (e.g. Moyano et al. 2022). Therefore, one or several other angular momentum transport mechanism must be acting in stellar interiors to explain the slow core rotations. Many additional transport mechanisms have been proposed to alleviate this important tension. For instance, internal gravity waves (Pinçon et al. 2017) or mixed modes Belkacem et al. (2015) could extract angular momentum from the near-core region, but the former becomes inefficient in red giant stars and the latter may be efficient enough only in late red giant stages.

Large-scale magnetic fields are promising candidates, because they can transport angular momentum via Maxwell torques. This new ingredient must be all the more important as recent asteroseismic studies demonstrated the presence of strong magnetic fields in red giants (Li et al. 2023; Hatt et al. 2024). However, the nature of these magnetic fields remains an open question. They could have a fossil origin, that is formed during the star formation or via core convective dynamo in the early stages, but too strong magnetic fields would produce a uniform rotation which is in tension with asteroseismic observations. Or, the magnetic fields could be generated by magnetohydrodynamic (MHD) instabilities in the stably stratified shear flows, which may trigger dynamo action. The instability can be either driven by differential rotation — magnetorotational instability (MRI, e.g. Jouve et al. 2020; Meduri et al. 2024) — or by strong currents — instability of the toroidal magnetic field (Tayler instability, e.g. Tayler 1973).

The dynamo driven the Tayler instability, the so-called Tayler-Spruit dynamo, was first theorised by Spruit (2002) and then revised by Fuller et al. (2019), providing scaling laws for the magnetic fields and transports. While this dynamo has remained elusive for a long time, the first numerical evidence of its existence was recently published (Petitdemange et al. 2023; Barrère et al. 2023). In the continuation of these studies, we present new numerical results demonstrating the existence of a new branch of the Tayler-Spruit dynamo.

[1] Département d'Astronomie, Université de Genève, Chemin Pegasi 51, 1290 Versoix, Switzerland
[2] Max Planck Institute for Gravitational Physics (Albert Einstein Institute), D-14476 Potsdam, Germany

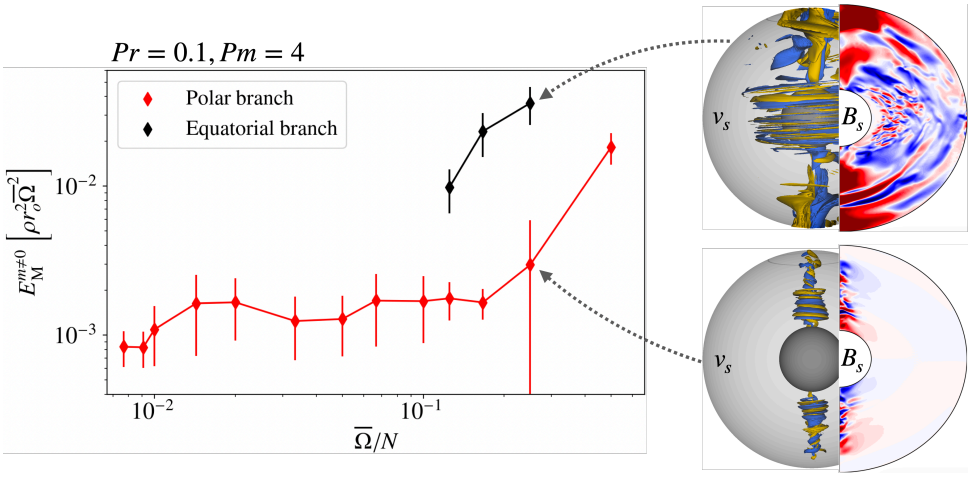

Fig. 1. Left: Bifurcation diagram representing the time and volume-averaged magnetic energy associated to the non-axisymmetric modes in rotational units as a function of the ratio $\overline{\Omega}/N$. The errorbars represent the standard deviation when the quantity is time-averaged. **Right:** 3D representations of the cylindrical radial velocity isocontours and meridional slices of the cylindrical radial magnetic field. The upper and bottom plots are a snapshots of the equatorial and dipolar Tayler-Spruit dynamos at $N/\overline{\Omega} = 4$, respectively.

2 Methods

We chose to model a stellar radiative region as a rotating stably stratified fluid. The fluid evolves according the MHD equations, which are solved using the pseudo-spectral code MagIC (Gastine & Wicht 2012; Schaeffer 2013) in a spherical configuration. To filter the acoustic waves, we chose the Boussinesq approximation, which assumes a uniform density profile. While this approximation ignores the density gradient present in stars, it makes the parametric study of the dynamo easier. Future numerical studies will investigate the influence of the density gradient.

The different thermal and magnetic diffusivities (κ and η, respectively) and the viscosity (ν) are treated explicitly using the thermal and magnetic Prandtl numbers $Pr \equiv \nu/\kappa = 0.1$ and $Pm \equiv \nu/\eta = 4$. The rotation and the stable stratifications are characterised by the Ekman number

$$E \equiv \frac{\nu}{d^2\overline{\Omega}} \in [1 \times 10^{-5},\, 6.5 \times 10^{-5}]\,, \tag{2.1}$$

and the Rayleigh number

$$Ra \equiv \frac{d^4 N^2}{\nu\kappa} \in [-4 \times 10^{11},\, -4 \times 10^{9}]\,, \tag{2.2}$$

where $d \equiv r_0 - r_i$ is the difference between the outer and inner radii, N is the Brunt-Väisälä frequency, and $\overline{\Omega}$ is the average rotation rate, which corresponds to the rotation at the radius $0.8r_o$. Varying E and Ra allows us to span a large interval of the ratio $N/\overline{\Omega} = \sqrt{RaE^2/Pr} \in [2, 130]$.

The differential rotation is imposed by adding a background azimuthal velocity field, to which the azimuthal velocity relaxes in a timescale noted $\tau^{-1} = (10 \times E)^{-1}$. Since we span a range of $Pr(N/\overline{\Omega})^2 \in [0.4, 1690]$, we impose a background field corresponding to shellular rotation profile, which seems appropriate (Philidet et al. 2020) and the rotation rate decreases with the radius. This volumetric forcing differs from the previous numerical simulations of the Tayler-Spruit dynamo, which force the differential rotation using fixed rotation rates on the spherical boundaries and so are prone to spherical Taylor-Couette instabilities.

3 Results

3.1 Bistable Tayler-Spruit dynamos

The simulations at $N/\overline{\Omega} = 2$ and $N/\overline{\Omega} = 4$ was initialised with a purely poloidal magnetic field with either a $(\ell, m) = (1, 0)$ (dipole) or a $(\ell, m) = (2, 0)$ (quadrupole) geometry and a strength $\sim 10^{-3}\,[(4\pi\rho r_o^2\overline{\Omega}^2)^{1/2}]$, which

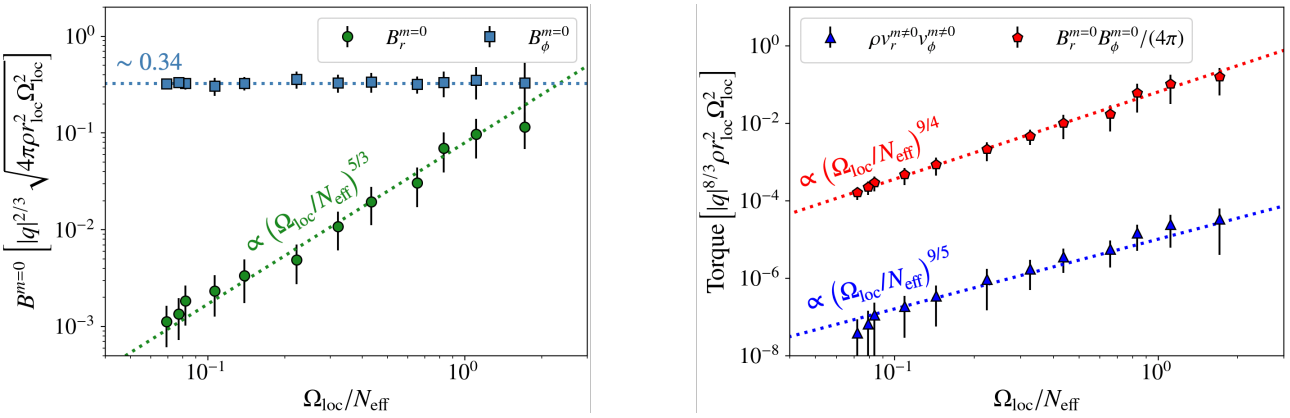

Fig. 2. Left: Axisymmetric radial and azimuthal magnetic fields in rotational units as a function of $\Omega_{\rm loc}/N_{\rm eff}$. The errorbars represent the standard deviation when the quantity is time-averaged. **Right:** Same as on the left but for the Reynolds (blue) and Maxwell (red) torques.

is $\sim 5-6$ times weaker than the saturated poloidal strength. From the obtained dynamos, we continued the dynamo branches at larger $N/\overline{\Omega}$ by starting from the previous saturated dynamo states. As illustrated in the bifurcation diagram of Fig. 1, we obtain two distinct dynamos, both driven by the Tayler instability. On the one hand, the quadrupole field triggered the dynamo with turbulence and a large-scale field at the equator, hence the name 'equatorial dynamo'. This solution is very similar to the one identified by Petitdemange et al. (2023), but is not maintained above $N/\overline{\Omega} \gtrsim 8$. On the other hand, the magnetic dipole activates a new Tayler-Spruit dynamo close to the polar axis, as identified by Barrère et al. (2023) in the case of proto-magnetars. The dynamo remains self-sustained until $N/\overline{\Omega} \sim 110$ and a long transient can be maintained up to stratifications around $N/\overline{\Omega} \sim 130$, which is a stratification regime not reached before.

3.2 Scaling laws

Since the simulations of the polar Tayler-Spruit dynamo span a wide range of $\overline{\Omega}/N$, we can obtain scaling laws for the magnetic field and the induced transport to quantify the impact on stellar physics. To measure the different quantities, we first calculate time and latitudinally-averaged radial profiles for each of them, and then average in an interval of radii containing half of the magnetic energy associated to the radial magnetic field. Using this method, we also define a local rotation rate $\Omega_{\rm loc}$, shear rate $q \equiv r/\Omega\, d_r\Omega$, and the local radius $r_{\rm loc}$ is the radius at the peak of radial magnetic energy. Finally, to include the mitigating effect of diffusivities on the stratification, we use the effective Brunt-Väisälä frequency $N_{\rm eff}^2 \equiv Pr/Pm \times N^2$.

Fig. 2 displays the scaling laws fitting the axisymmetric magnetic fields (plot on the left) and the torques (plot on the right) as a function of $|q|$ and $\Omega_{\rm loc}/N_{\rm eff}$. For the magnetic fields, we obtain

$$B_\phi^{m=0} \sim 0.33\sqrt{4\pi\rho r_{\rm loc}^2}\,\Omega_{\rm loc}|q|^{2/3}\,, \tag{3.1}$$

$$B_r^{m=0} \sim 0.08\sqrt{4\pi\rho r_{\rm loc}^2}\,\Omega_{\rm loc}\left(|q|^2\frac{\Omega_{\rm loc}^5}{N_{\rm eff}^5}\right)^{1/3}\,. \tag{3.2}$$

While the radial magnetic field follows the analytical prescription of Fuller et al. (2019), the azimuthal component is only impacted by the shear and not by the stratification. As expected, the magnetic field is clearly dominated by its azimuthal component in the strongly stratified regime.

On the other hand, the torque induced by the Tayler-Spruit dynamo is dominated by the generated large magnetic as the Maxwell torque ($T_{\rm M}$) is 10^3-10^4 greater than the Reynolds torque ($T_{\rm R}$). The scaling laws fitting our data read

$$T_{\rm M} \equiv \frac{B_r^{m=0}B_\phi^{m=0}}{4\pi} \sim 0.06\,\rho r_{\rm loc}^2\,\Omega_{\rm loc}|q|^{8/3}\left(\frac{\Omega_{\rm loc}}{N_{\rm eff}}\right)^{9/4}\,, \tag{3.3}$$

$$T_{\rm R} \equiv \rho v_r^{m\neq0}v_\phi^{m\neq0} \sim 1.2\times10^{-5}\,\rho r_{\rm loc}^2\,\Omega_{\rm loc}|q|^{8/3}\left(\frac{\Omega_{\rm loc}}{N_{\rm eff}}\right)^{9/5}\,. \tag{3.4}$$

$T_{\rm M}$ is therefore slightly less efficient than predicted by Fuller et al. (2019) because of the prefactor and the power of $\Omega_{\rm loc}/N_{\rm eff}$, which is 2.25 instead of 2 in Fuller et al. (2019). Note that the measured $T_{\rm M}$ does not follow the scaling law obtained if we simply multiply Eqs 3.3 and 3.4. This can be explained by the fact that the $B_r^{m=0}$ and $B_\phi^{m=0}$ does not have the same distribution in the integrated volume, showing the importance of being in 3D and a limit of 1D and one-zone models. Interestingly, $T_{\rm R}$ follows a scaling law similar to the Maxwell torque, disregarding the difference in the prefactor.

We can use these laws to obtain physical values of these quantities for stellar interior. Here, we focus on the case of the hydrogen-burning shell in red giants, which are extremely stratified due to a strong chemical composition gradient. $N_{\rm eff}/\Omega_{\rm loc}$ peaks around $10^3 - 10^4$ in this region, which gives, assuming $|q| \sim 1$, $B_r^{m=0} \approx 0.006 - 0.3\,{\rm G}$ and $B_\phi^{m=0} \approx 10^5\,{\rm G}$. We therefore confirm that $B_r^{m=0}$ is several order of magnitude weaker than the field measured in red giants, but the strong $B_\phi^{m=0}$ may have an impact on asteroseismic signal (e.g. Dhouib et al. 2022). Finally, the diffusivity associated to T_M reads $T_{\rm M}/(\rho|q|\Omega_{\rm loc}) \approx 10^3 - 2\times10^5\,{\rm cm^2\,s^{-1}}$, which is in agreement with the diffusivity needed in 1D stellar models to match the observed rotation of red giant and red clump stars (Moyano et al. 2022).

4 Conclusions

In this work, we investigated a new solution of the Tayler-Spruit dynamo. Our results show that the dynamo can be sustained for stratifications up to $N/\overline{\Omega} \sim 130$. Despite an azimuthal magnetic field remaining very strong, the induced transport is less efficient than predicted by Fuller et al. (2019), even though much more than the branch of Petitdemange et al. (2023). Future implementations of the scaling laws we provide in stellar evolution models will show the consistency of the Tayler-Spruit dynamo with the recent measurements of surface and core rotations. Besides, this work fosters simulations using realistic density backgrounds from evolution models to test our results and conclusions. For asteroseismology, the existence of these two Tayler-Spruit dynamos with distinct radial magnetic field topologies predicts a variety of asymmetry parameter values, as already glimpsed by the observations (Li et al. 2023; Hatt et al. 2024). However, the magnetic field is dominated by the azimuthal component. Therefore, the assumption of a dominant radial component used by current detection methods is irrelevant for the Tayler-Spruit dynamo. This fosters the development of new asteroseismic diagnostics to detect magnetic fields produced by this dynamo in the future.

Thank you to the organizers of the SF2A 2025 and those of the session S20 for the opportunity to present this work.

References

Barrère, P., Guilet, J., Raynaud, R., & Reboul-Salze, A. 2023, MNRAS, 526, L88
Belkacem, K., Marques, J. P., Goupil, M. J., et al. 2015, A&A, 579, A30
Dhouib, H., Mathis, S., Bugnet, L., Van Reeth, T., & Aerts, C. 2022, A&A, 661, A133
Fuller, J., Piro, A. L., & Jermyn, A. S. 2019, MNRAS, 485, 3661
Gastine, T. & Wicht, J. 2012, Icarus, 219, 428
Gehan, C., Mosser, B., Michel, E., Samadi, R., & Kallinger, T. 2018, A&A, 616, A24
Hatt, E. J., Ong, J. M. J., Nielsen, M. B., et al. 2024, MNRAS, 534, 1060
Jouve, L., Lignières, F., & Gaurat, M. 2020, A&A, 641, A13
Li, G., Deheuvels, S., & Ballot, J. 2024, A&A, 688, A184
Li, G., Deheuvels, S., Li, T., Ballot, J., & Lignières, F. 2023, A&A, 680, A26
Li, G., Van Reeth, T., Bedding, T. R., et al. 2020, MNRAS, 491, 3586
Meduri, D. G., Jouve, L., & Lignières, F. 2024, A&A, 683, A12
Moyano, F. D., Eggenberger, P., Meynet, G., et al. 2022, A&A, 663, A180
Petitdemange, L., Marcotte, F., & Gissinger, C. 2023, Science, 379, 300
Philidet, J., Gissinger, C., Lignières, F., & Petitdemange, L. 2020, Geophysical and Astrophysical Fluid Dynamics, 114, 336
Pinçon, C., Belkacem, K., Goupil, M. J., & Marques, J. P. 2017, A&A, 605, A31
Schaeffer, N. 2013, Geochemistry, Geophysics, Geosystems, 14, 751
Spruit, H. C. 2002, A&A, 381, 923
Tayler, R. J. 1973, MNRAS, 161, 365